

Structural Modeling and Identification Using Neural Networks

F.Y. Hadaegh, R.Y. Chiang
Jet propulsion laboratory
California Institute of Technology
Pasadena, CA 91109

C-F. Lin, A.S. Politopoulos
American GNC Corporation
9131 Mason Ave.
Chatsworth, CA 91311

Submitted to the 1994 ACC

Keywords: Feedforward Neural Network, Hopfield Network, Large Space Structure

Abstract

This paper presents the use of a multilayer feedforward neural network and the Hopfield network to emulate and identify the dynamics of a reduced order model of a large space antenna-like ground experiment structure located at the JPL/AF-PL Large Spacecraft Control Laboratory. Input-output relations are shown to be closely replicated by a feedforward network and modal characteristics identified by a Hopfield network.

1. introduction

Neural networks can be used to emulate dynamical systems to facilitate both analysis and simulation [3], [4], [5], [6]. In particular, a multi-layer feedforward network [1] with sigmoidal activation functions can be configured to mimic the dynamic behavior of a given system. The representation capability of the neural network results from its ability to realize through training the input/output relations of the system. The training act determines the values of a set of weights such that the desired input/output relations result. A very important theoretical underpinning for such an approach is provided by recent work that shows that multi-layer neural networks can approximate any continuous mapping to any desired approximation error level.

Given a dynamic system a neural network can be used to model the system. The system determines a set of input/output pairs either experimentally or analytically derived. To effect neural modeling of the dynamic system a training record is generated by assembling the inputs and the corresponding outputs. The weights of the neural network are then adjusted in a supervised mode to nullify the error between the desired outputs and the output predictions of the neural network.

Although feedforward type artificial neural networks are well suited for successfully learning input-output mappings they are rarely studied as parameter estimators. This is due to the fact that a system's parameters can not be explicitly retrieved from a feedforward network's connection weights since the network learns only mapping functions.

On the contrary, one type of recurrent neural network, namely, the Hopfield network [2] (Figure 1) does not suffer from such a drawback. Thus, it can be used as a dynamic system's parameter estimator if one can create a direct correspondence of the architectural form of the Hopfield network to the dynamical structure of the problem at hand.

In the following sections the multilayer feedforward network is used for input-output mapping characterization and the Hopfield network for modal parameters estimation.

2. System Characterization

The model used in this paper is that of an antenna-like flexible structure, located at the JPL/AF-PL Large Spacecraft Control Laboratory. This model is summarized here for convenience with its details presented in Appendix A. The state space equation of the model is

$$\dot{x} = A_p x + B_p u \quad (1)$$

where A_p and B_p are the system matrices.

Table 1 shows the parametric values of this model. The output equation is given by

$$y = C_p x \quad (2)$$

with the output measurement matrix

$$C_p = [-0.0729 \quad -0.1959 \quad -0.04495 \quad 0.2706 \quad 0.1164 \quad 0 \quad 0 \quad 0 \quad 0 \quad 0]$$

3. Multilayer Feedforward Network Modeling

A three-layer feedforward neural network with 60 nodes in each hidden layer is used to model the above dynamics. The neural elements in the first two layers have a sigmoidal activation whose outputs lie between -1 and 1. The output layer utilizes linear neurons so that scaling of the outputs can be avoided. Backpropagation is used to train the multilayer network.

The ability of the network to learn arbitrary mappings is demonstrated by Figures 2 through 7. Figure 2 shows the evolution in training of a desired map between a 100 element input vector and a 100 element output vector. The input has a sinusoidal

$$u = \cos(0.1 k) \quad 1 \leq k \leq 100 \quad (3)$$

form while the desired output is nonlinear (i.e. with harmonics present)

$$y = \cos(0.1 k) + \sin(0.2 k) + \sin(0.3 k) \quad (4)$$

At each epoch, the training data (i.e., the desired output, represented by solid lines and the corresponding input) are presented to the network. The predictions of the network (dashed

lines) are compared with the desired output. The error between the two is used to adjust the network weighting. Initially, the network weights are assumed to be random. The learning history plots show the error as the square root of the sum-of-the-squares of the difference between the actual and predicted output up to the epoch silo\;']1. Occasionally, there is a loss of memory in the training as evidenced by the presence of a spike in the learning history plot. This is due to zigzagging behavior of the gradient based error minimization search. A good match is observed after 200 training iterations.

Figures 8 through 13 show the network's ability to learn input output relations directly relevant to the JPL model. An input function lasting for 0.5 sees and consisting of the superposition of sinusoids

$$u = 0.03 * \cos(10 t) + 0.015 \sin(20 t) + 0.08 * \cos(30 t) \quad (5)$$

is constructed and the response of the JPL model to this function is noted. The input and output functions are sampled every 5 insecs. The neural network is then trained to yield the same output function as the system for the identical input function. It is seen from the Figure that after 200 iterations the agreement between the neural network's response and the actual system's output is very close.

4. Structural identification Using a Hopfield Network

In this section an on-line identification scheme using the Hopfield network is used to estimate the modal parameters of the reduced order JPL Model without prior knowledge, assuming that the system states and their time derivatives are available.

4.1 Circuit Dynamics of the Hopfield Network

The dynamic equations of an analog Hopfield network model can be described as [2],

$$\begin{aligned} C_i \, dU_i/dt &= \sum_{j=1}^N T_{ij} V_j - U_i/R_i + J_i \\ V_i &= g(\lambda_i U_i) \\ U_i &= (1/\lambda_i) g^{-1}(V_i) \quad , 1 \leq i \leq N \end{aligned} \quad (6)$$

where N is the total number of neurons, T_{ij} is the connection strength between neuron i and j , C_i is the i -th neuron capacitance, and R_i, J_i are the i -th neuron impedance and bias input, respectively. The input-output relation between the i -th neuron state U_i and output V_i is determined by the activation function $g(x)$, where $g(x)$ is a nonlinear sigmoid function. The dynamics of (6) are influenced by both the learning rate λ_i and the activation function $g(x)$. For instance, in the high learning rate limit case, $\lambda \rightarrow \infty$ and $g(x)$ approaches a step function.

The network's Lyapunov function E , for either synchronous or asynchronous update in the state of the neurons is:

$$E = -1/2 \sum_{i=1}^N \sum_{j=1}^N T_{ij} V_i V_j - \sum_{i=1}^N J_i V_i + (1/\lambda) \sum_{i=1}^N (1/R_i) \int_0^{V_i} g^{-1}(V) dV \quad (7)$$

E is also called the computational energy of the network. By using symmetric network connection strengths $T_{ij} = T_{ji}$ and $g(x)$ a monotonically increasing sigmoid function, Hopfield demonstrated that the time evolution of V_i will change in the direction such that the energy function E decreases.

4.2 Hopfield Based Neural Estimator Network

The state of the neurons can be confined to positive hypercubes G_i where G_i is defined as $G_i > 1$, $G_i \in \mathbf{R}^+$ for $1 \leq i \leq N$. This approach is explained as follows. By using the sigmoid activation function $g(x) = \tanh(x)$ for the neurons, the input-output relation of each neuron can be defined by

$$\begin{aligned} V_i &= G_i \tanh(\lambda_i U_i) \\ U_i &= -1/(2 \lambda_i) \ln \left(\frac{G_i - V_i}{G_i + V_i} \right), \quad 1 \leq i \leq N \end{aligned} \quad (8)$$

where the output of each neuron, V_i , is constrained within the subset of positive hypercubes G_i . Therefore, with the network states representing the dynamical system's parameters, \hat{p} , the hypercube limits, G_i , must be chosen such that $|\hat{p}| < |G_i|$.

With the input-output relation for each neuron defined by (8), the analog Hopfield network dynamics (6), when operated in the high impedance and unit capacitance conditions, can be described purely in terms of the neuron output state variable V_i by substituting U_i of (8) into (6) as follows:

$$dU_i/dt = (\partial U_i / \partial V_i) (dV_i/dt) \quad (9)$$

where $\partial U_i / \partial V_i$ is given as

$$(\partial U_i / \partial V_i) = \frac{(G_i / \lambda_i)}{(G_i + V_i)(G_i - V_i)} \quad (10)$$

Hence, the dynamic equations of the resulting neural network can be formulated as

$$\begin{aligned} \dot{V} &= K (T V + I) \\ K &= \text{diag.} [k_i] \\ k_i &= \left[\frac{\lambda_i (G_i + V_i) (G_i - V_i)}{G_i} \right], \quad 1 \leq i \leq N \end{aligned} \quad (11)$$

where N is the total number of neurons, V is an $N \times 1$ column vector containing the network output, and K is a diagonal matrix consisting of non-negative diagonal elements. Comparing (11) and (6), it is noted that the neural network based estimator architecture of (11) has preserved the primary structure of the analog Hopfield model defined in (6) as well as the advantages of representing the system parameters directly without scaling.

In the case of a high-gain limiting condition where $\lambda_i \rightarrow \infty$, the corresponding network computational energy E and its time derivative \dot{E} are given by

$$\begin{aligned} E &= -(1/2 V^T T V + I V) \\ dE/dt &= (\partial E / \partial V) \dot{V} \\ &= -(T V + I)^T K (T V + I) \leq 0 \end{aligned} \quad (12)$$

where $()^T$ indicates the transpose of a matrix. It is noted that the time derivative of the network's computational energy \dot{E} in (12) can be shown to be always non-positive, which means that time evolutions of the state of neuron V_i stops at an equilibrium point, where

$$dE/dt \leq 0, \text{ and } dE/dt = 0 \rightarrow dV/dt = 0 \quad (13)$$

since E is a Lyapunov function of the system (11).

4.3 Design of the Hopfield Based Neural Estimator

The block diagram of the estimation scheme is depicted in Figure 14. Let the continuous time state space equation of the actual system be given as

$$\dot{x} = A_p x + B_p u \quad (14)$$

where A_p and B_p are the actual system matrices, respectively, x is the state variable, and u is the control actuation. Denoting by A_s and B_s the unknown adjustable system matrices, the estimation error for a series-parallel estimation scheme can be written as

$$\begin{aligned} \dot{y} &= A_s x + B_s u - K e \\ e &= x - y \end{aligned} \quad (15)$$

The dynamic equation of the estimation error e is

$$\dot{e} = (A_p - A_s) x + (B_p - B_s) u + K e \quad (16)$$

or

$$\dot{e} = \dot{x} - (A_s x + B_s u) + K e \quad (17)$$

The objective is to minimize the time rate of change of the error, i.e., \dot{e} . More specifically, the minimization criterion is the error energy function

$$E = (1/h) \int_0^h (1/2) \dot{e}^T \dot{e} dt \quad (18)$$

However, the term $K e$ in (17) introduces a dependency of \dot{e} on y (since $e = x - y$) which in turn depends on A_s and B_s . This leads to a complicated energy surface E whose global minimum may not be directly accessible. q'bus, K is set to zero and E becomes a quadratic function of A_s and B_s

$$\begin{aligned} E &= (1/h) \int_0^h (1/2) \dot{e}^T \dot{e} dt \\ &= (1/h) \int_0^h (1/2) (\dot{x} - A_s x - B_s u)^T (\dot{x} - A_s x - B_s u) dt \\ &= (1/h) \left((1/2) \text{tr} A_s < x, \dot{x} > + (1/2) \text{tr} B_s < u, \dot{x} > + \right. \\ &\quad \left. \text{tr} A_s < x, u^T > B_s^T - \text{tr} A_s < x, \dot{x}^T > - \text{tr} B_s < u, \dot{x}^T > + \right. \\ &\quad \left. (1/2) < \dot{x}^T, \dot{x} > \right) \end{aligned} \quad (19)$$

$$\begin{aligned}
B_p &= \begin{bmatrix} \mathbf{0}, & 0, & \dots & \mathbf{0} \\ h, & b_{1,2}, & \dots & b_{1,r} \\ 0, & 0, & \dots & 0 \\ b_{2,1}, & b_{2,2}, & \dots & b_{2,r} \\ \mathbf{0}, & \mathbf{0}, & \dots & \mathbf{0} \\ & & & \\ b_{J,1}, & b_{J,2}, & \dots & b_{J,r} \end{bmatrix} \\
&= \left[\begin{array}{cccc} 0 & B_1^T & 0 & B_2^T \dots 0 & B_k^T \dots 0 & B_J^T \end{array} \right]^T
\end{aligned}$$

where $x_k = \begin{bmatrix} q_k & \dot{q}_k \end{bmatrix}^T$ is the state vector, ω_k and ζ_k is the natural frequency and modal damping associated with the k -th mode, respectively. $A_k = \{a_{e,g}\}$, $1 \leq k \leq J$, is a 2 by 2 matrix associated with the k -th mode and $a_{e,g}$ is the entries of A_k for $1 \leq e, g \leq 2$. The modal gain matrix corresponding to the k -th mode is defined as $B_k = \{b_{p,s}\}$ where B_k is of dimension 1 by r and $b_{p,s}$ is the entry of B_k associated with the k -th mode for $1 \leq s \leq r$, $1 \leq p \leq J$.

The state of the neurons V represents different elements in the A_p and B_p matrices as follows:

$$\begin{aligned}
V &= \left[V^{(1)T}, \dots, V^{(k)T}, \dots, V^{(J)T} \right]^T \\
V^{(k)} &= [a_{1,1}, \dots, a_{2,2}, 0, 0, \dots, 0, b_{1,1}, \dots, b_{1,r}]^T
\end{aligned} \tag{22}$$

The network computational energy (18) is

$$\begin{aligned}
E &= (1/h) \int_0^h (1/2) \dot{e}^T \dot{e} dt \\
&= (1/h) \int_0^h (1/2) (\dot{x} - A_s x - B_s u)^T (\dot{x} - A_s x - B_s u) dt \\
&= (1/h) [(1/2) \text{tr} A_s \langle x, x^T \rangle + A_s^T + (1/2) \text{tr} B_s \langle u, u^T \rangle + B_s^T + \\
&\quad \text{tr} A_s \langle x, u^T \rangle + B_s^T - \text{tr} A_s \langle x, \dot{x}^T \rangle - \text{tr} B_s \langle u, \dot{x}^T \rangle + \\
&\quad (1/2) \langle \dot{x}^T, \dot{x} \rangle] \\
&= (1/2) \sum_{k=1}^J \text{tr} [A_k \langle x_k, x_k^T \rangle + A_k^T + B_k \langle u, u^T \rangle + B_k^T + \\
&\quad 2A_k \langle x_k, u^T \rangle + B_k^T - 2A_k \langle x_k, \dot{x}_k^T \rangle - 2B_k \langle u, \dot{x}_k^T \rangle] + \\
&\quad (1/2) \langle \dot{x}^T, \dot{x} \rangle \\
&= - \sum_{k=1}^J [1/2 V^{(k)T} \hat{T}^{(k)} V^{(k)} + \hat{T}^{(k)T} V^{(k)}] + (1/2) \langle \dot{x}^T, \dot{x} \rangle \\
&= -(1/2 V^T T V + T^T V) + (1/2) \langle \dot{x}^T, \dot{x} \rangle
\end{aligned} \tag{23}$$

The connection strength matrix T in 23 is a block diagonal matrix given by

$$T = \text{blockdiag. } \mathbf{i}^{(1)}, \dots, \mathbf{i}^{(k)}, \dots, \hat{T}^{(J)} \quad , 1 \leq k \leq J \tag{24}$$

Mode Number	1	2	3	4	5	6	7
Modal Frequency (rad/sec)	0.	0.	0.	17.5	23.5	59.5	60.8
Modal Damping	0.	0.	0.	0.3%	0.3%	0.3%	0.3%

Table 1: Modal Characteristics of The Reduced Order Model.

and $\hat{T}^{(k)}$ is the connection strength matrix associated with the k -th mode, which is determined by

$$\hat{T}^{(k)} = (-1/h) \int_0^h [T^{(k)}] dt \quad (25)$$

$$T^{(k)} = \begin{bmatrix} x_k & x_k^T & 0 & 0 \\ 0 & x_k & x_k^T & x_k u^T \\ 0 & u & x_k^T & u u^T \end{bmatrix}$$

where the dimension of $T^{(k)}$ depends on the state measurements x_k , the time derivatives \dot{x}_k , as well as on the control variable u . Accordingly, the bias input weight matrix I can be formulated as follows:

$$I = [\hat{j}^{(1)T}, \dots, \hat{j}^{(k)T}, \dots, \hat{j}^{(J)T}]^T \quad (26)$$

with $\hat{j}^{(k)}$ is defined as

$$\hat{j}^{(k)} = (1/h) \int_0^h [q_k \dot{q}_k \ddot{q}_k \ q_k \ q_k \dot{q}_k \ \dot{q}_k \dot{q}_k \ \ddot{q}_k \ u^T]^T dt \quad (27)$$

Hence, for a space structural system consisting of J modes, with r input channels, the dimension of the neural estimator network connection strengths matrix, T , is $J(4+r) \times J(4+r)$, the bias input weight matrix, I , is $J(4+r) \times 1$, and the state of neurons, V , is $J(4+r) \times 1$, respectively.

4.5 On-Line Simulation

On-line estimation of the modal parameters of the JPL model are conducted by implementing (11). Between each sampling period, the state of the neurons, V , evolves to minimize the network computational energy and thus the system parameters (natural frequencies, ω_k , modal damping ratio, ξ_k , and modal gains, B_k , ($1 \leq k \leq J$) associated with each mode), being identical to the neural network state elements, are the converged values.

In demonstrating/validating the efficacy of this proposed neural estimation scheme, the JPL reduced order model is employed. This reduced model preserves the principal dynamics of the system. The mode] corresponds to the 5 flexural modes listed in Table 1. One flexural mode has a damping ratio of 0.12 and the remaining flexural modes have a damping ratio of 0.01.

4.6 Simulation Results

The Hopfield network is trained to identify the modal parameters (Table 1) with a single input. The system state variable, its time derivative and the control signal are contaminated with zero mean white noise.

In simulating a high gain limiting case, a large learning rate is used for each neuron with $\lambda_i = 2.0e+4$, $i = 1, 2, \dots, 56$. The state of the neurons evolves within the prescribed hypercubes where the size of the hypercubes is chosen as $G_i = 1.0e+4$, $i = 1, 2, \dots, 30$. The upper bound, 30, represents the total number of states for the neural net since there are 5 modes and 6 states per mode (4 corresponding to the modal dynamics and 2 to the gain matrix). The capacitance is chosen as $C_i = 1.0e+4$, $i = 1, 2, \dots, 30$. Moreover, the initial state of all neurons is assigned as -] 0.0 except for those associated with the natural frequency where positive initial values were assigned in complying with the physical structural model. The initial guess of the natural frequencies corresponding to each mode is assigned as 10 rad/sec.

The results depicted in Figures 15 through 21 show the estimated by the Hopfield network parameters versus their true values with the input to the network signals (i.e., the state variables, their time derivative and the control actuations) contaminated by noise.

5. Conclusions

This paper presented examples showing the successful application of neural networks to structural modeling and identification. The powerful properties of neural networks can thus be utilized to aid the modeling of dynamic systems for either control or simulation applications.

6. Acknowledgement

This work was partially performed at the Jet Propulsion Laboratory, California Institute of Technology under contract with the National Aeronautics and Space Administration.

References

- [1] D.E. Rumelhart and J.J. McClelland, editors, "Parallel Distributed Processing" *MIT Press*, 1986.
- [2] J.J. Hopfield, "Neurons with graded responses have collective computational properties like those of two-state neurons" *Proceedings of the National Academy of Science, USA*, pages 3088-3092, 1982.
- [3] D. Boussalis, S.J. Wang, "Neural Network Vibration Control based on output feedback." *Proceedings of the IEEE Regional Conference on Aerospace Control Systems*, pages 48-52, 1993.
- [4] Jet Propulsion laboratory, "Flexible structure control laboratory development and technology demonstration. Final Report to U.S. Air Force Astronautics laboratory and National Aeronautics and Space Administration, Oct. 1, 1987.
- [5] C.C. Ih, D.S. Bayard, S.J. Wang, D.B. Eldred, "Adaptive Control Experiment with a Large Flexible Structure" *Proceedings of the 1988 AIAA Conference*, pages 832-851, 1988.
- [6] C.C. Ih, D.S. Bayard, A. Ahmed, S.J. Wang, "Experimental Study of Robustness in Adaptive Control for Large Flexible Structures" *Journal of Guidance Control and Dynamics*, pages 1-20, January-February 1993.

Appendix A: System Dynamics Model

The model used for this paper is a large space shuttle-like ground experiment structure located at the JPL/AF-PL Large Spacecraft Control Laboratory (LSC/L). A finite element model for this structure has been developed by JPL personnel.

Description of the Experiment Structure

Configuration

A schematic diagram of the shuttle-like structure is depicted in Figure 22. The main component of the apparatus consists of a central hub to which 12 ribs are attached. The diameter of the dish structure is 18.5 feet, the large size being necessary to achieve the low modal frequency desired. The ribs are coupled together by two rings of pretensional wires. Functionally, the wires provide coupling motion in the circumferential direction which cannot be provided by the hub. The ribs are each supported at two locations along their free length by levitators. Each levitator assembly consists of a pulley, a counterweight, and a wire attached to the counterweight which passes over the pulley and attaches to the rib. The hub is mounted to the backup structure through a gimbal platform, so that it is free to rotate about two perpendicular axes in the horizontal plane. A flexible boom is attached to the hub and hangs below it, and a feed mass, simulating the feed horn of an antenna, is attached at the free end of the boom. The boom for our current experiment is 3-foot long.

Actuators

Each rib can be individually excited or controlled by a rib-root actuator. Each rib-root actuator has a solenoid design which reacts against a mount that is rigidly attached to the hub. In addition two hub actuators are provided to torque the hub about its two gimbal axes. The hub torques do not provide torque directly, but rather are linear force actuators which provide torque to the hub by pushing at its outer circumference. The torque provided is equal to the force times the lever arm about the axis of rotation. The placement of these actuators guarantees good controllability of all of the flexible modes of motion. The location of the actuators are shown in Figure 23.

Sensors

The sensor locations are also shown in Figure 23. First each of the 24 levitators is equipped with an incremental optical encoder which measures the relative angle of the levitator pulley. The levitator sensors thus provide, in an indirect manner, the measurement of the vertical motion of the corresponding ribs at the points where the levitators are attached. There are also four evenly spaced linear variable differential transformers (LVDT) rib-root sensors collocated with four rib-root sensors. The hub angular positions are measured by two rotary variable differential transformers (RVDT) mounted directly at the gimbal bearings. Note that each hub sensor measures the structural response to the actuator mounted orthogonal to itself. Hence, although the actuator/sensor pairs HA1/HS1 and HA10/HS10 are physically

collocated, it is $HA1/HS10$ and $HA10/HA1$ that are collocated in the sense of "dual" variables about a common axis.

Dynamic Model

The system modes can be obtained using finite element analysis. Each rib, and the boom, is divided into IO beam-type elements and the hub is modeled as a very stiff plate. The normal modes and their frequencies can be obtained by solving a generalized eigenvalue problem in standard form:

$$Kx = \omega^2 Mx$$

where K is the stiffness matrix, M is the mass matrix, and x is the eigenvector with frequency ω

The symmetry of the structure makes it possible to separate variables and write the circular dependence of a given mode shape by inspection. For a given mode, the displacement of the i th rib is given by ,

$$\text{displacement of } i\text{-th rib} = \frac{2\pi ik}{n} \cos(\frac{2\pi ik}{n} - \phi)$$

where n is the number of ribs, and ϕ is a phase angle determined by the coordinate system transformation. Here k is a circular wave number associated with a given mode.

Mode shapes of the structure can be grouped according to their circular wave number k , which range from $k = 0$ to $k = 6$. Solutions with $k = 0, 2, 3, 4, 5$ and 6 are symmetric about the hub, in the sense that all reaction forces on the hub caused by the ribs exactly cancel out. In such modes, which are called "dish modes", neither the hub nor the boom participates in modal motion. On the other hand, modes in which $k = 1$ are asymmetric with respect to reaction forces on the hub. These modes, which are called "boom dish modes", involve motion of the boom, hub and dish structures together. The lower frequency modes are listed in Table 1 and Table 2, respectively.

Mode No.	Boom-dish modes		k
	Axis 4-10 Subsystem	Axis 1-7 Subsystem	
1	0.091	0.091	1
2	0.616	0.628	1
3	1.685	1.687	1
4	2.577	2.682	1
5	4.558	4.897	1
6	9.822	9.892	1

Table 2: Normal Boom-Dish Modes

A finite element model consisting of the first 30 flexible modes, 6 actuator inputs, and 30 sensor measurements is provided by JPL. Only six sensor outputs will be used for our investigation. The available sensors and actuators are listed in Table 3 and Table 4, respectively.

Dish modes		
	Frequency (Hz)	k
	0.210-	0
2	0.253*	2
3	0.290"	3
4	0.322*	4
5	0.344"	5
6	0.351	6
7	1.517	0
8	1.533*	2
9	1.550"	3
10	1.566"	4
11	1.578*	5
12	1.583	6
13	4.656	0
14	4.658"	2
15	4.660*	3
16	4.661*	4
17	4.662*	5
18	4.663	6
19	9.474	0
20	9.474"	2
21	9.474*	3
22	9.474*	4
23	9.474*	5
24	9.474	6

* two-fold degenerate modes

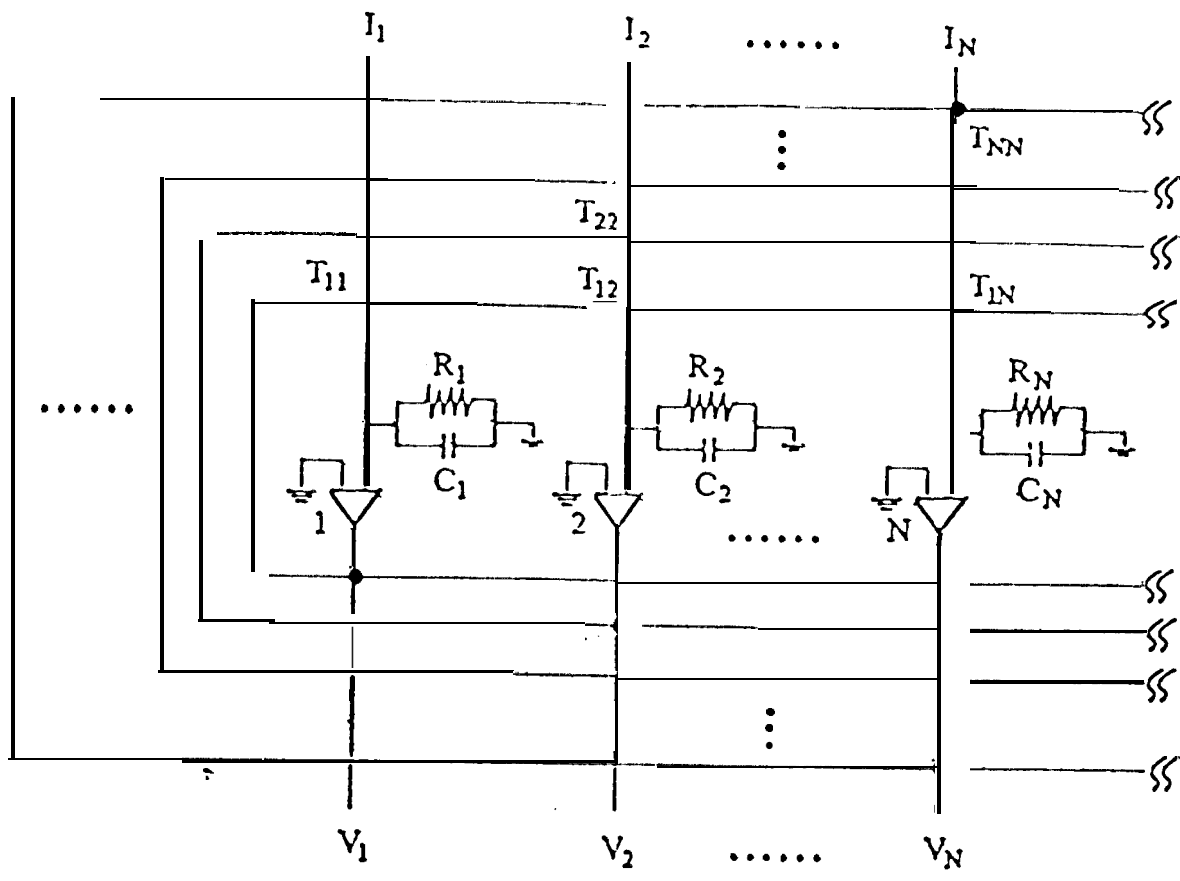
Table 3: Normal Dish Modes

Index Number	Actuator
1	RA1 Rib root actuator at rib No. 1
2	RA4 Rib root actuator at rib No. 4
3	RA7 Rib root actuator at rib No. 7
4	RA10 Rib root actuator at rib No. 10
5'	HAIO Hub actuator about rib 4-10 axis
6	11A] Hub actuator about rib 1-7 axis

Table 4: Available Actuators

Index Number	Sensor
1 - 12	Inner levitated rib displacement sensors I11 - I12
13 - 24	Outer levitated rib displacement sensors O1 - O12
5	HS1 Hub rotation sensor (about rib 1 - 7 axis)
26	HS10 Hub rotation sensor (about rib 4 - 10 axis)
27	RS1 Rib root displacement sensor at rib No. 1
28	RS4 Rib root displacement sensor at rib No. 4
29	RS7 Rib root displacement sensor at rib No. 7
30	RS10 Rib root displacement sensor at rib No. 10

Table 5: Available Sensors



- | | |
|------------------------------|------------------|
| V_i Neuron State | I_i Bias Input |
| C_i Capacitance | R_i Resistance |
| T_{ij} Connection Strength | V Amplifier |

Figure 1. Schematic of the Hopfield Neural Network

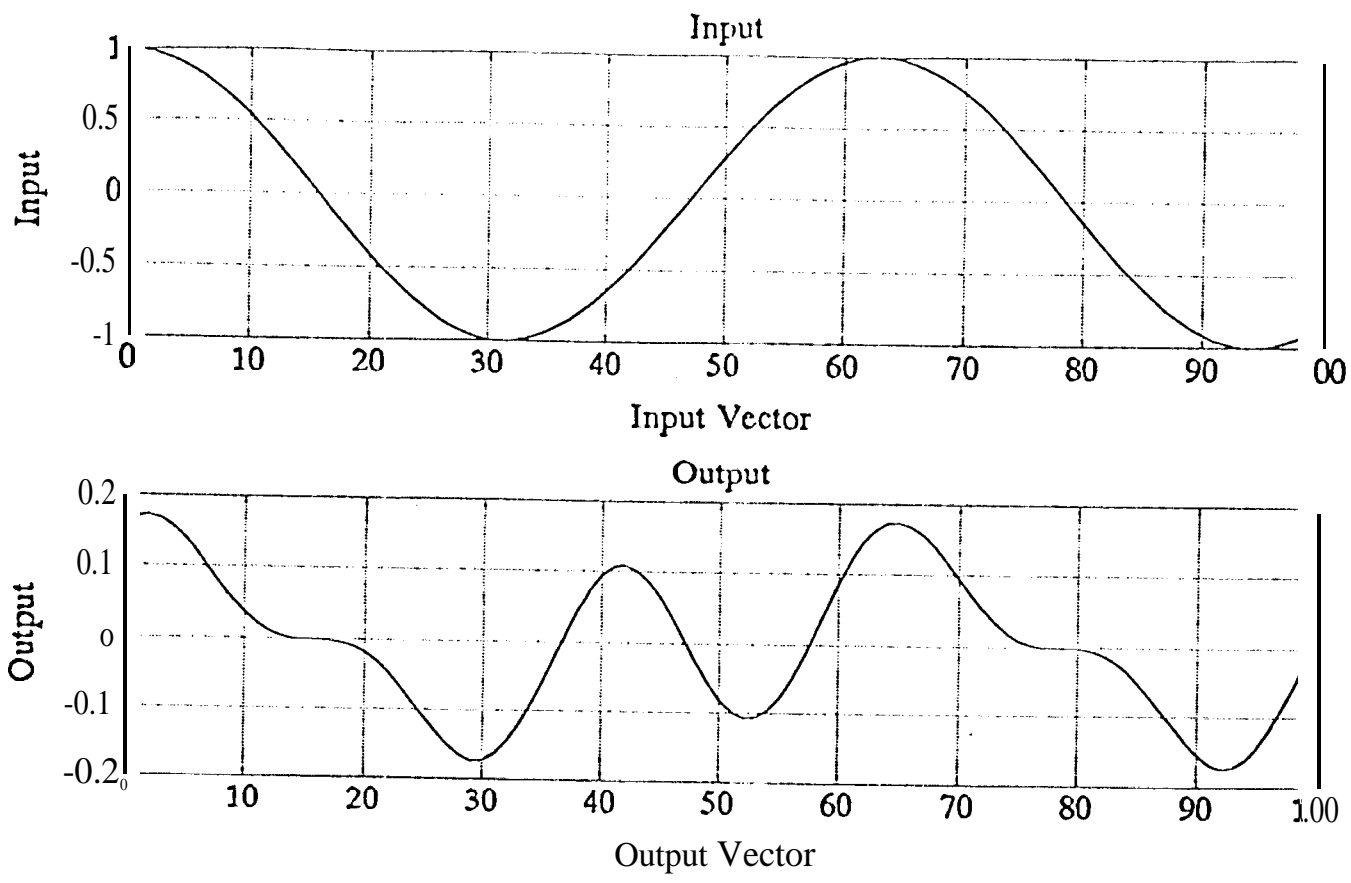


Figure 2. An Arbitrary Input-Output Relation

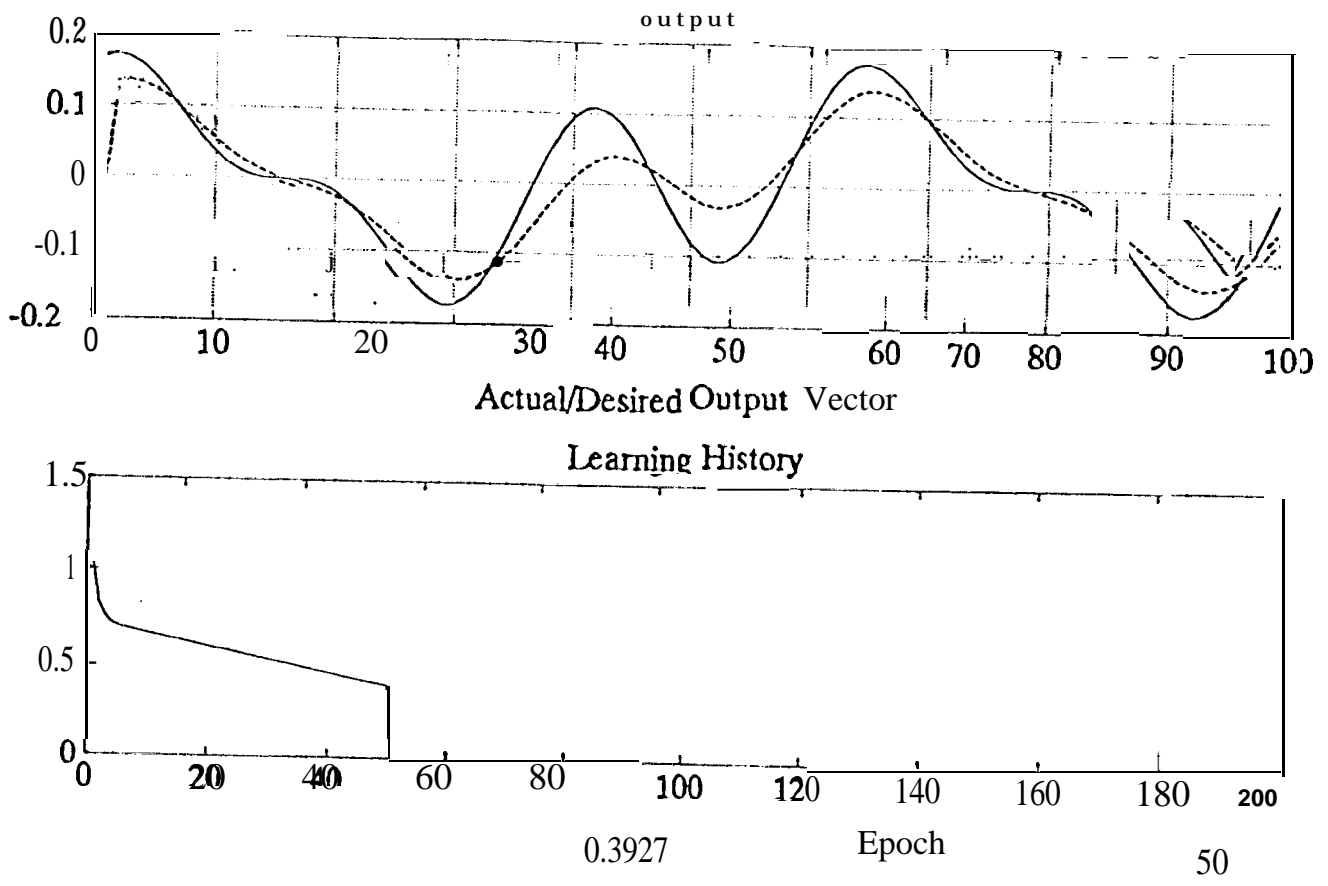


Figure 4. Training of the multilayer neural network, 50th epoch.

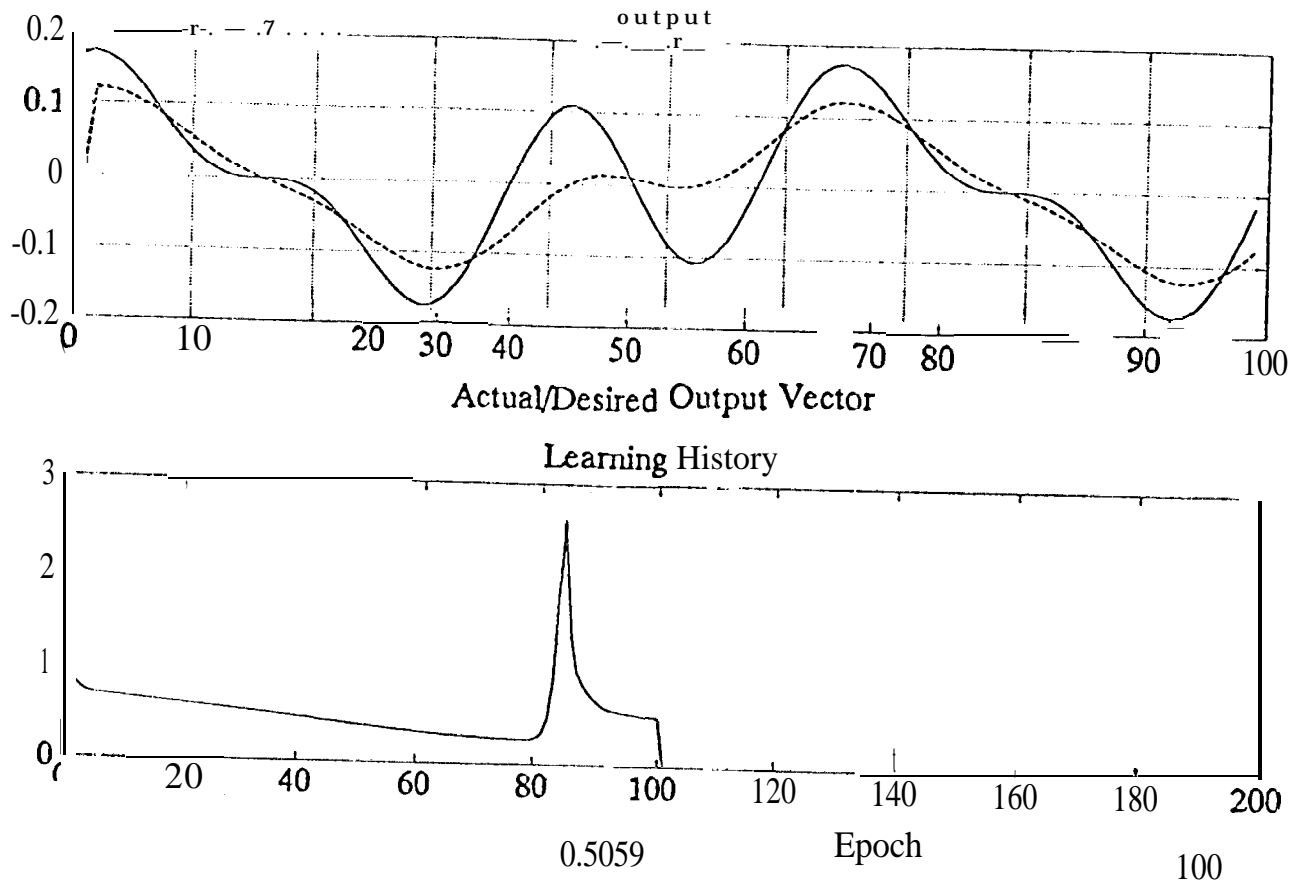


Figure 5. Training of the multilayer neural network, 100th epoch,

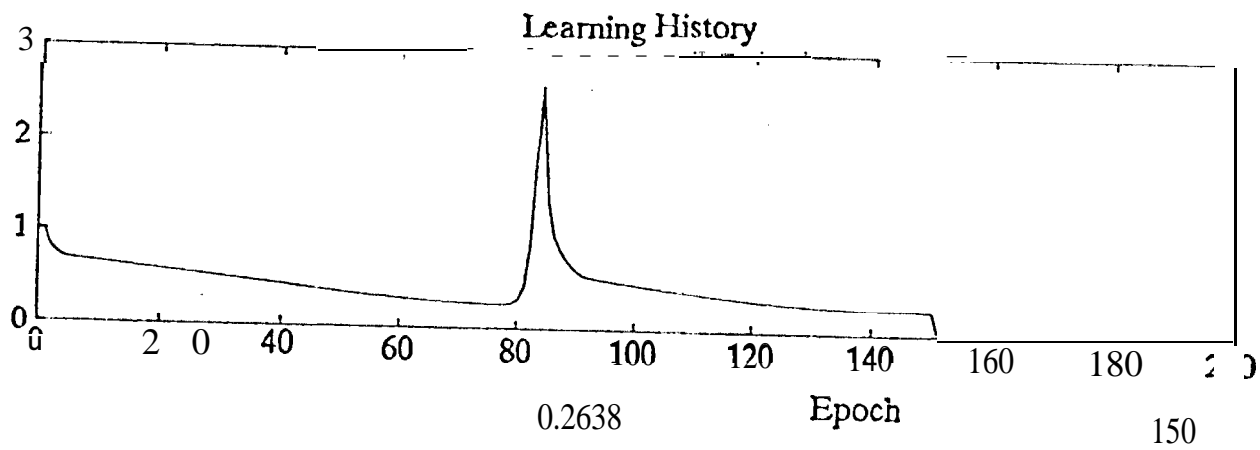
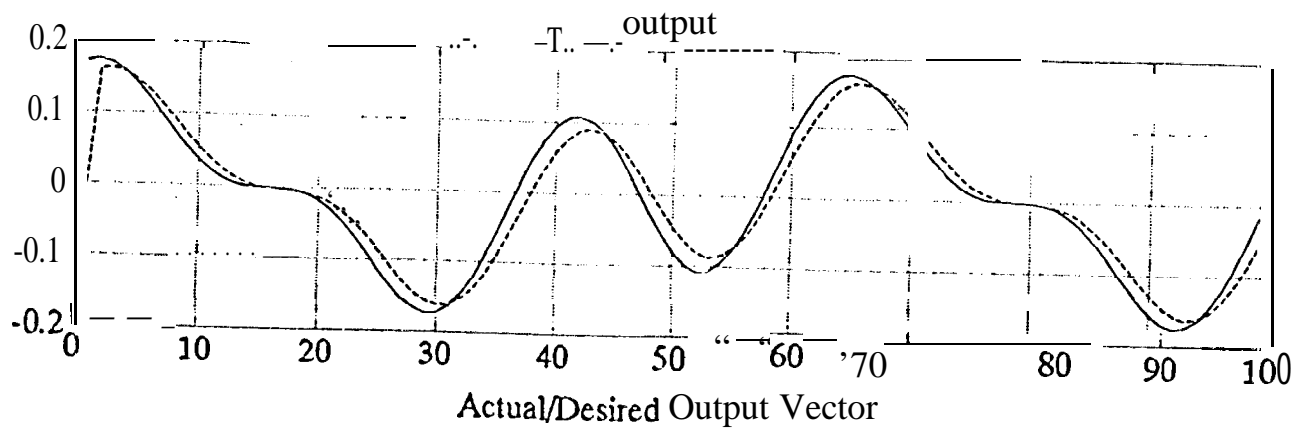


Figure 6. Training of the multilayer neural network, 150th epoch.

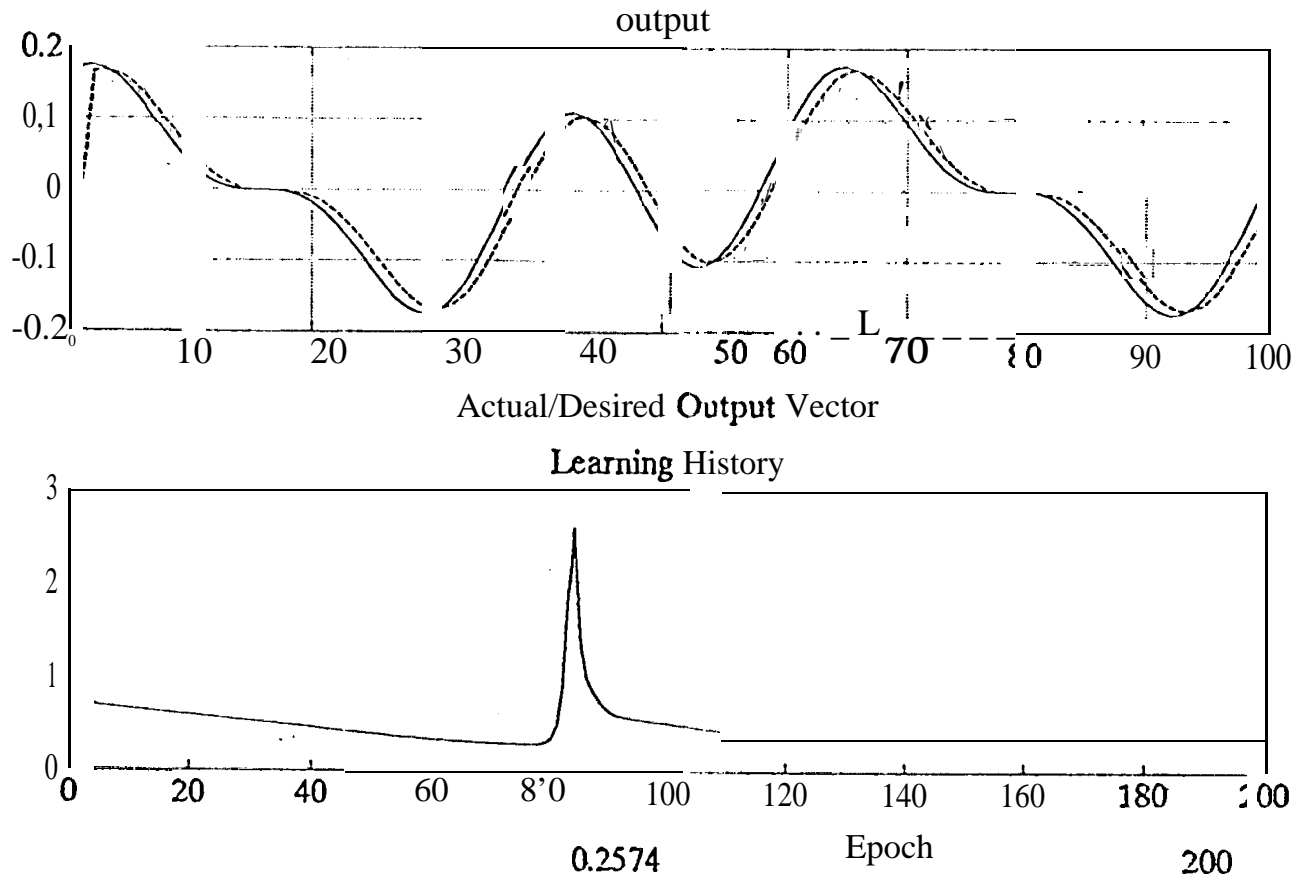


Figure 7. Training of the multilayer neural network, 200th epoch.

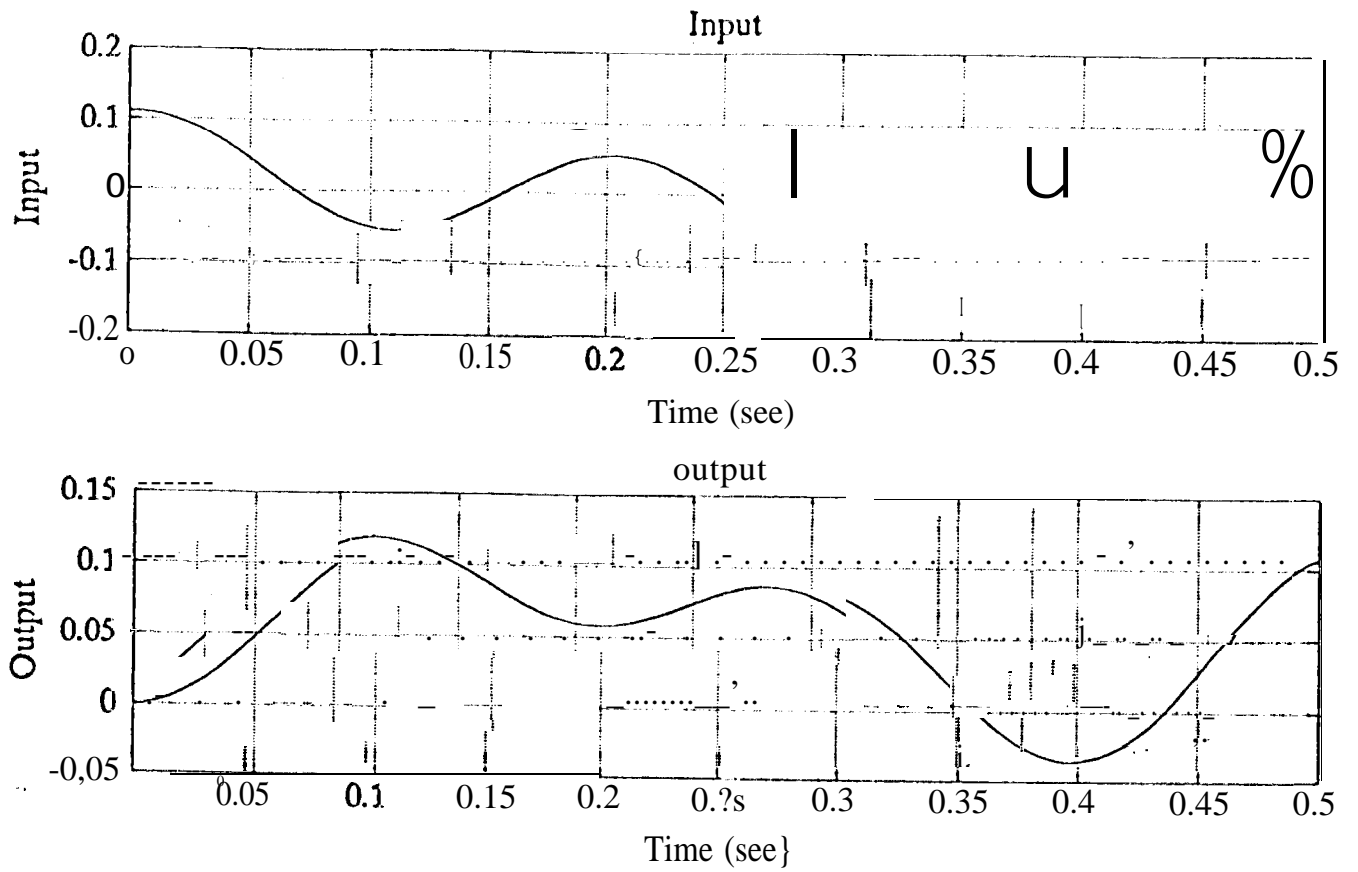


Figure 8. Input-Output Relation for the JPL ModelSystem.

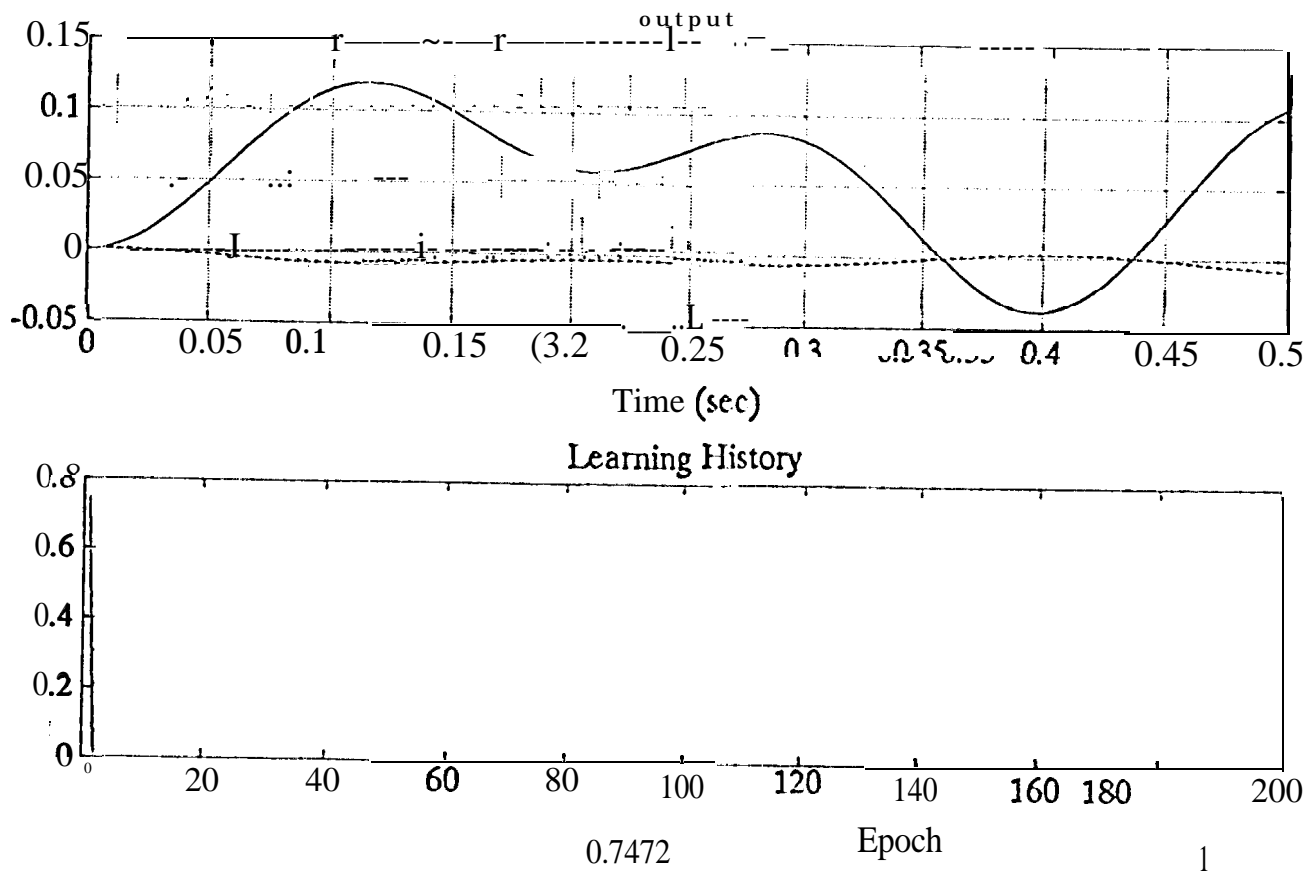


Figure 9. Training of the multilayer neural network, 1st epoch.

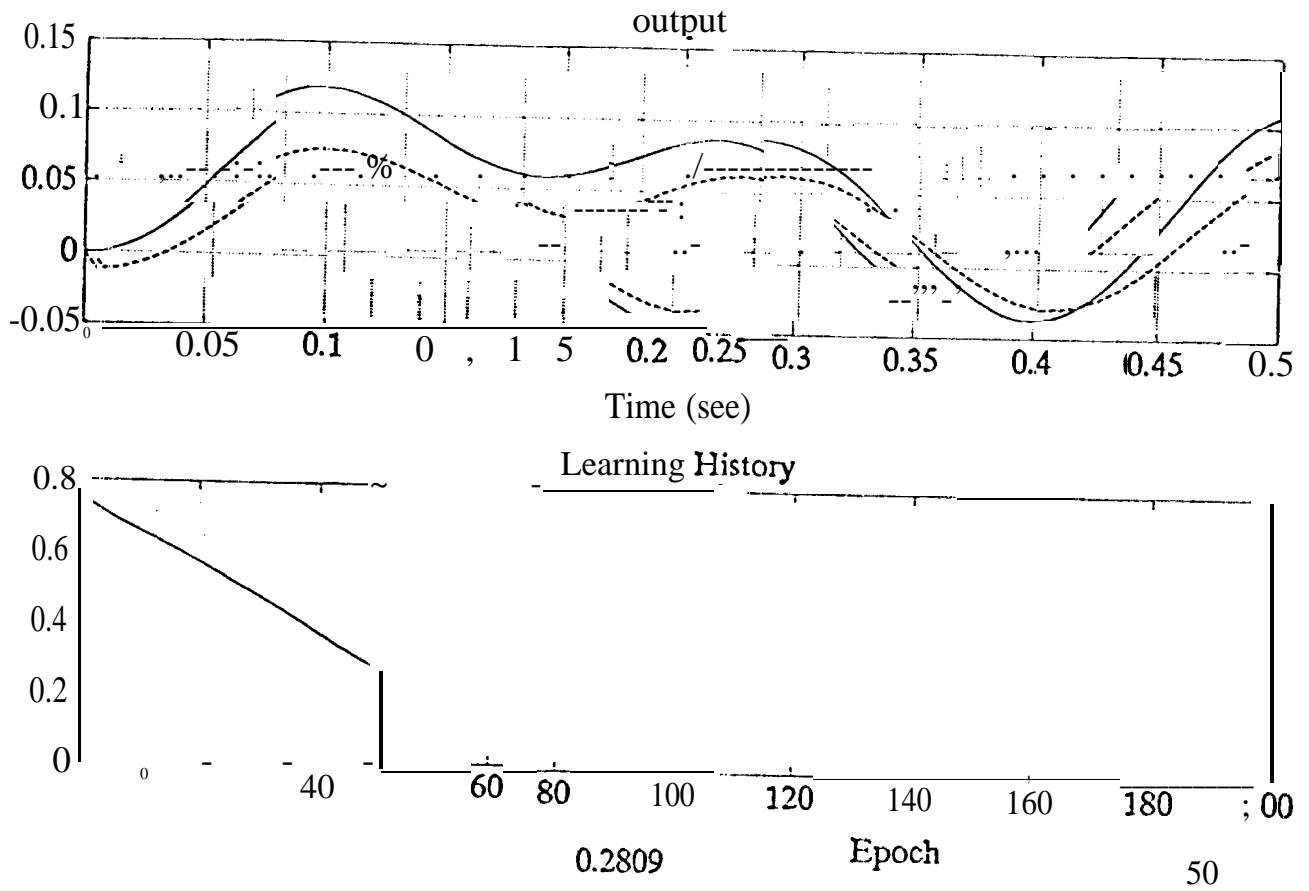
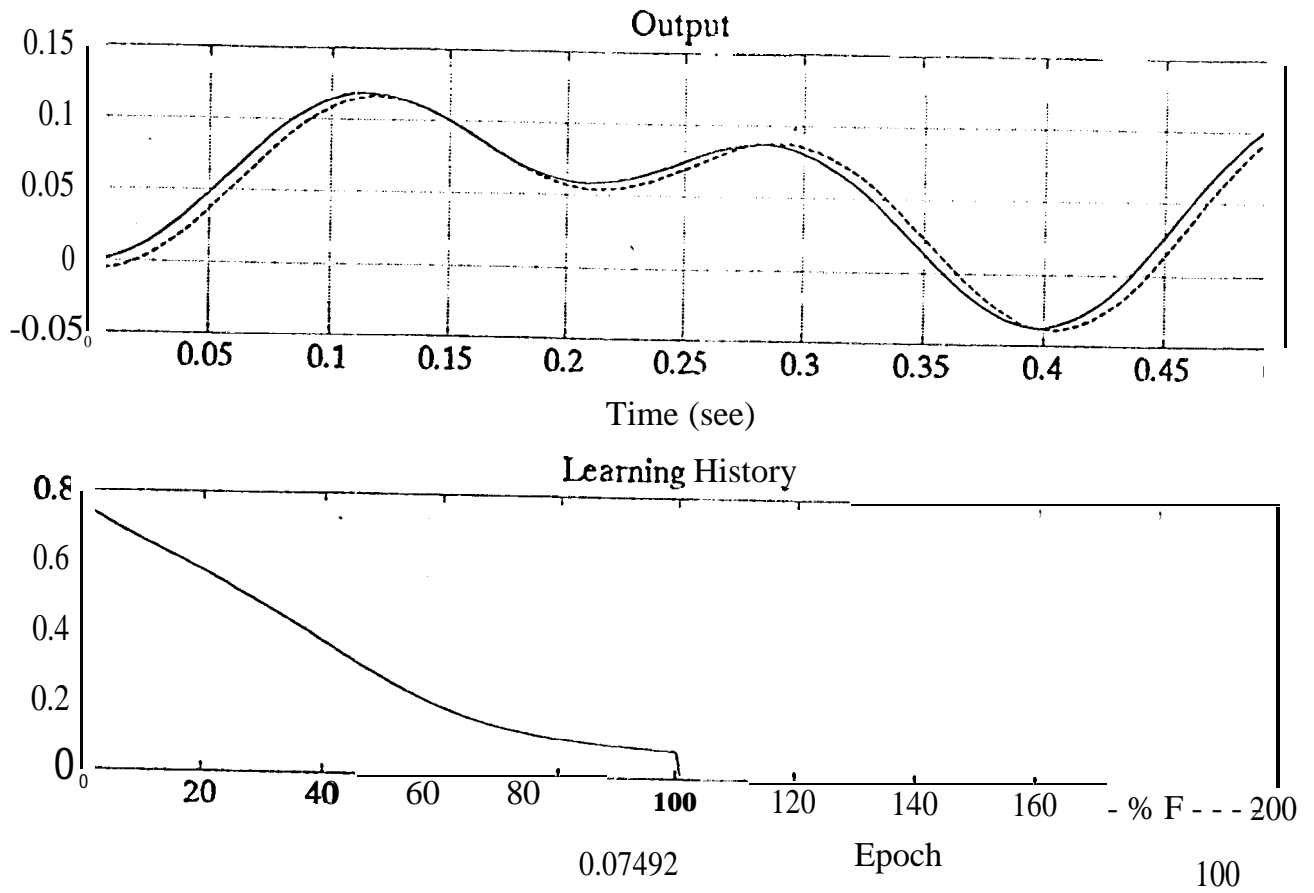


Figure 10. Training of the multilayer neural network, 50th epoch.



Figure; 11. Training of the multilayer neural network, 100th epoch.

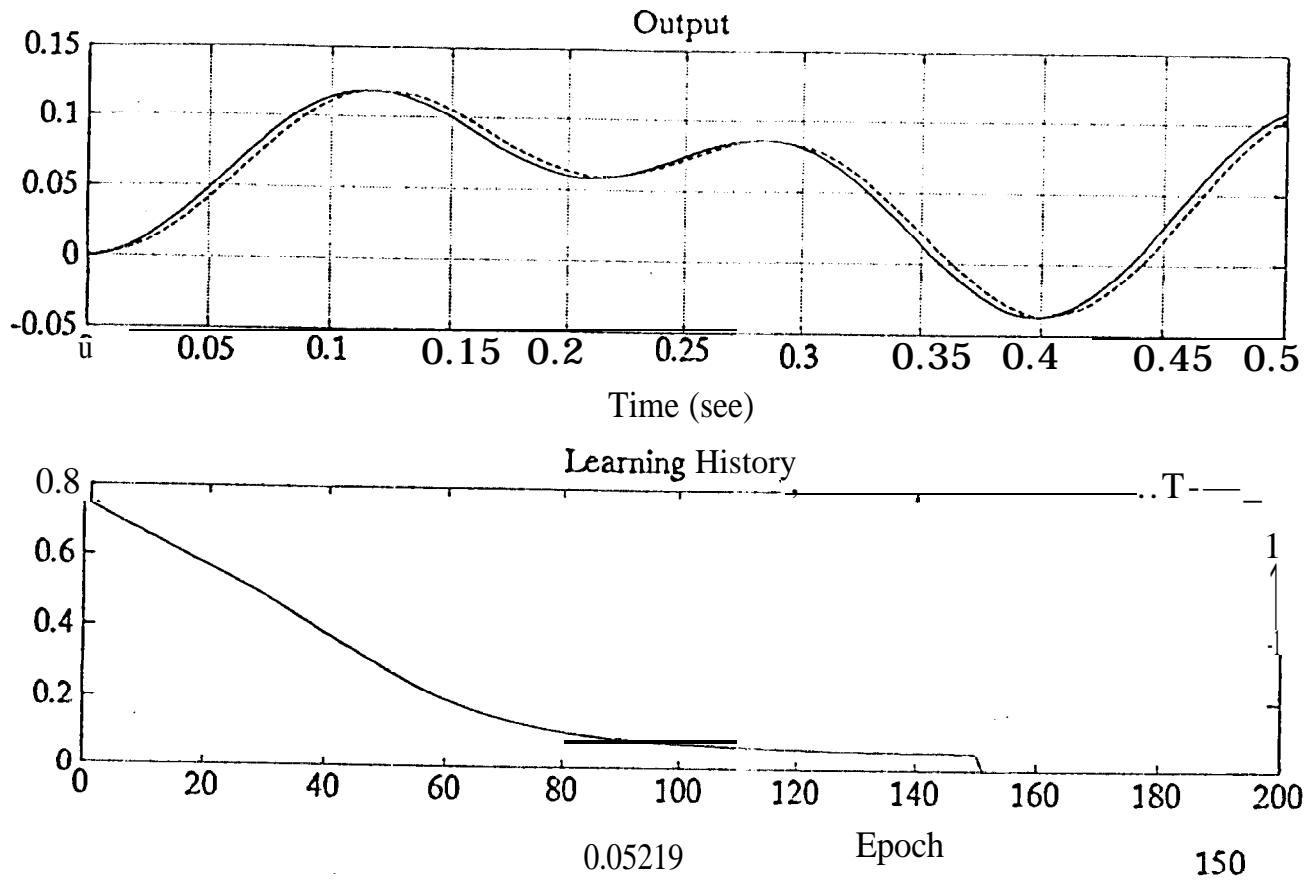


Figure 12. Training of the multilayer neural network, 150th epoch.

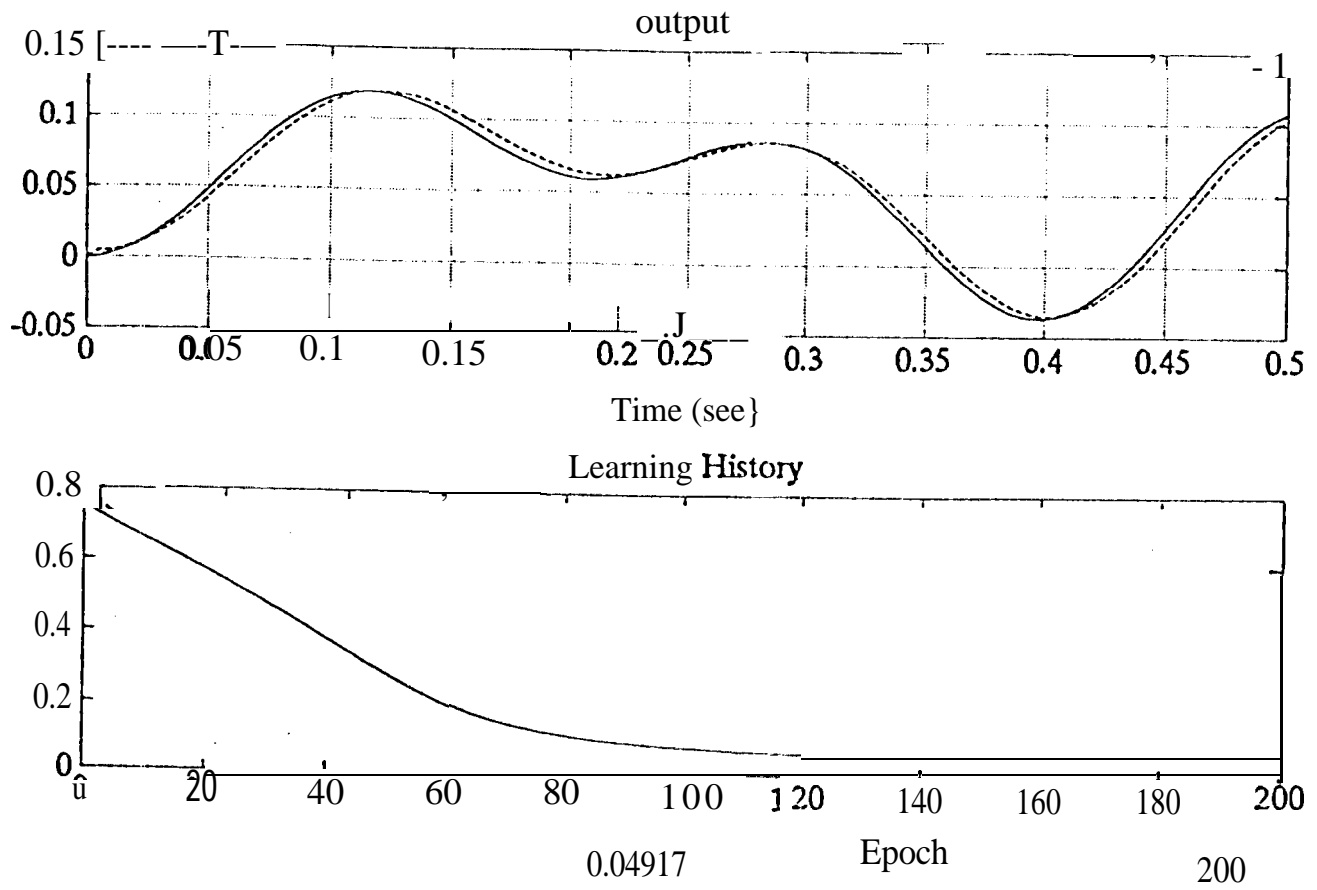


Figure 13. Training of the multilayer neural network, 200th epoch.

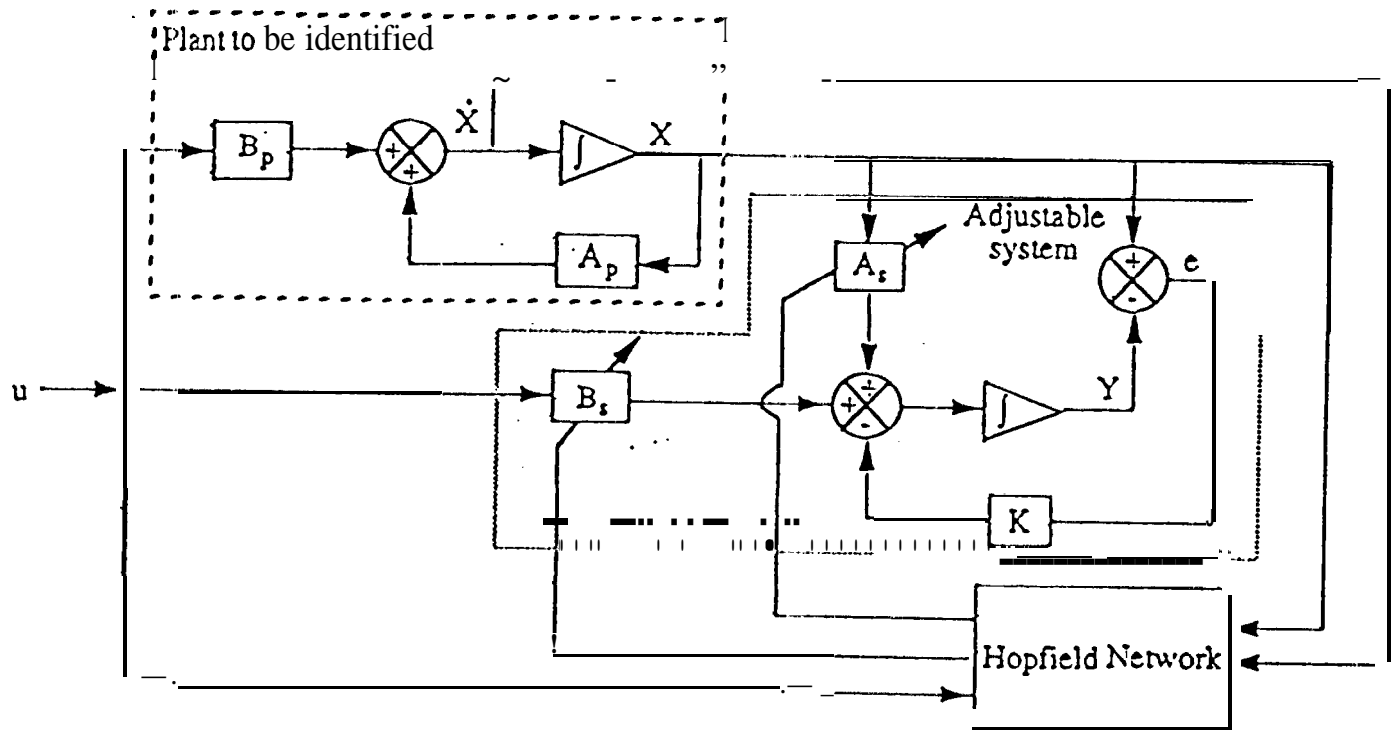


Figure 14. Parametric Estimation Scheme Using a Hopfield Neural Network.

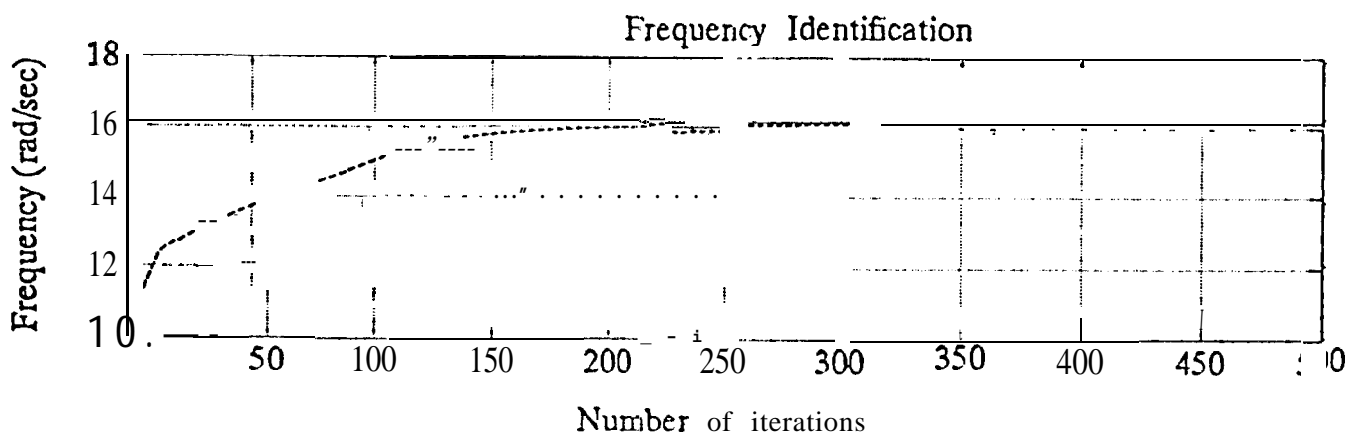


Figure 15. Estimated 4th Modal Frequency of the Reduced Order System.

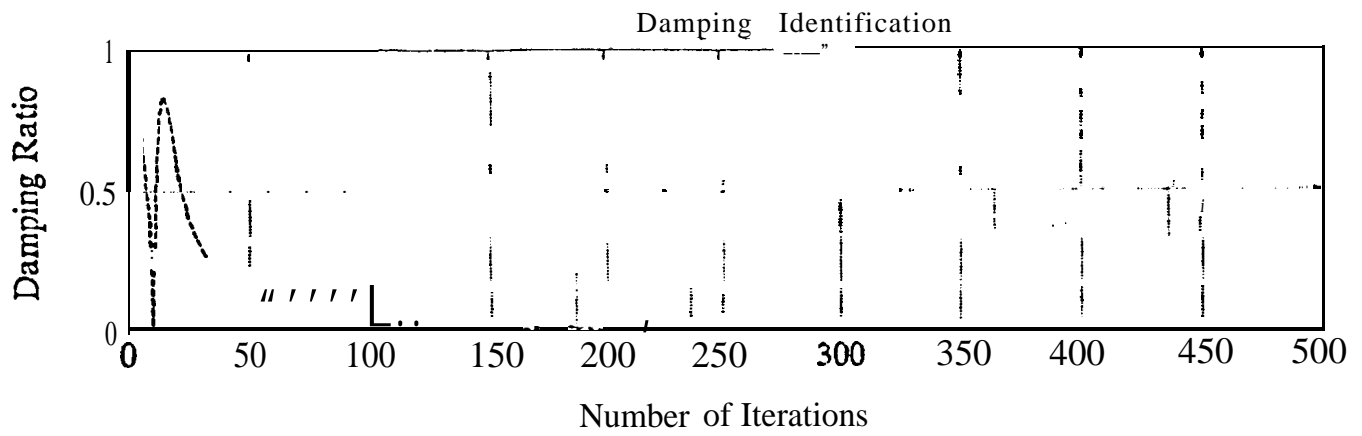


Figure 16. Estimated 4th Modal Damping of the Reduced Order System.

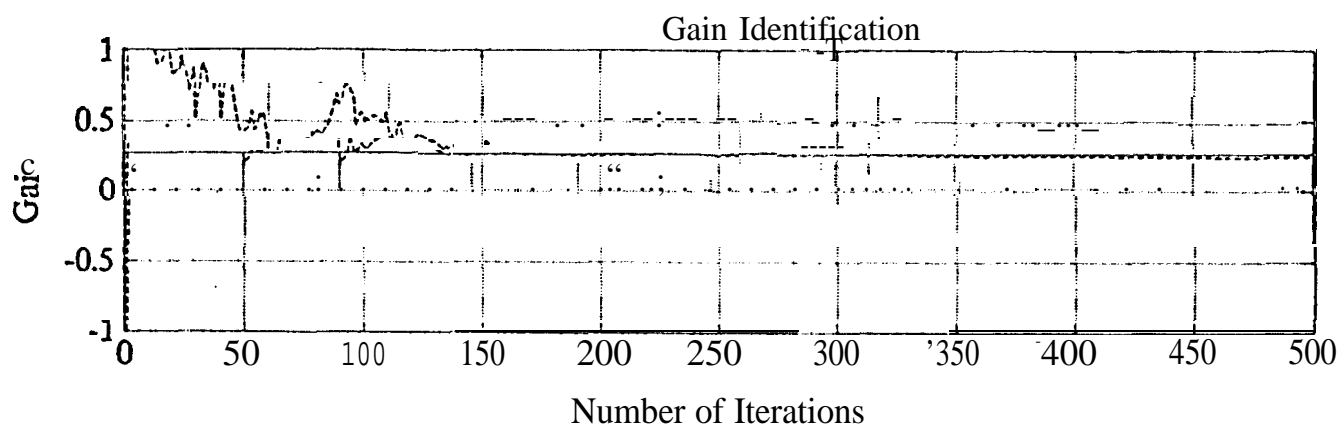


Figure 17. Estimated 4th Modal Gain of the Reduced Order System,

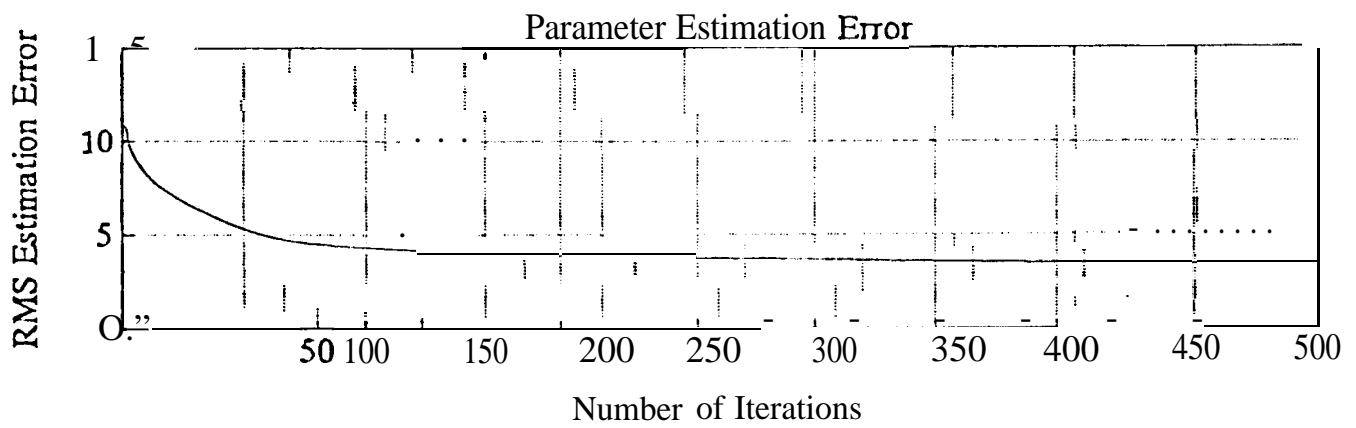


Figure 17. RMS Value of 4th Modal Parameter Estimation Error.

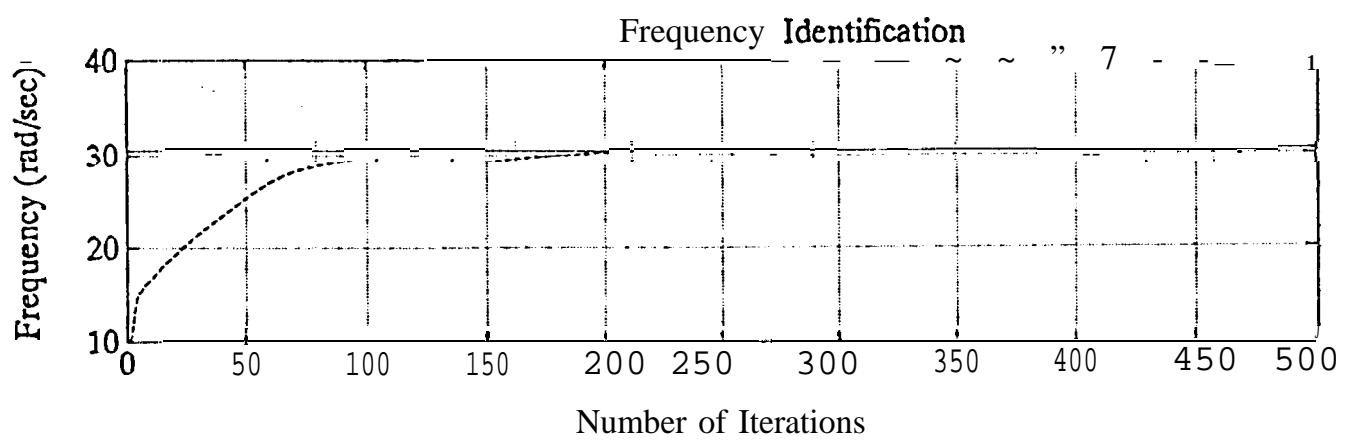


Figure 18. Estimated 5th Modal Frequency of the Reduced Order System.

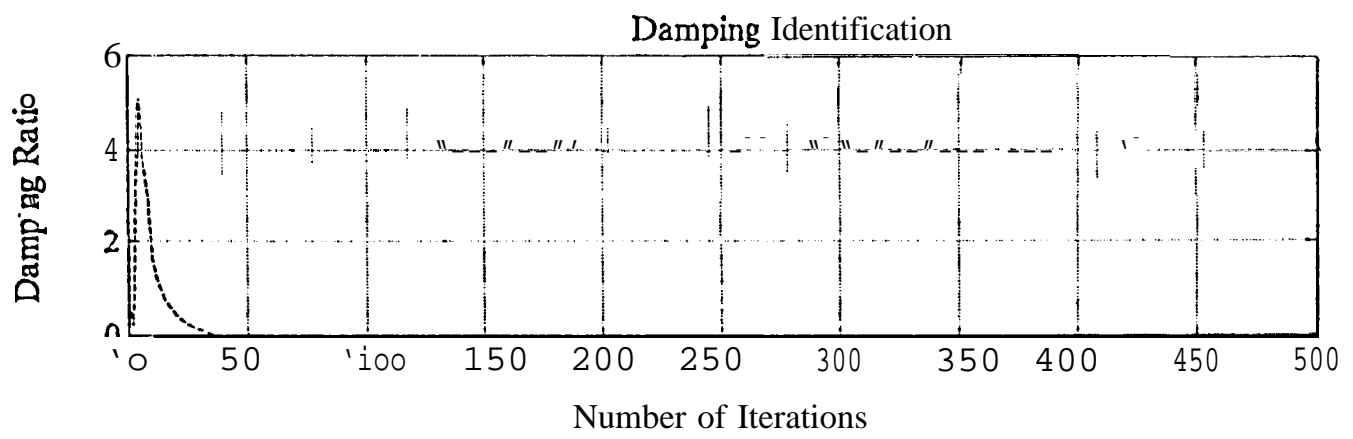


Figure 19. Estimated 5th Modal Damping of the Reduced Order System.

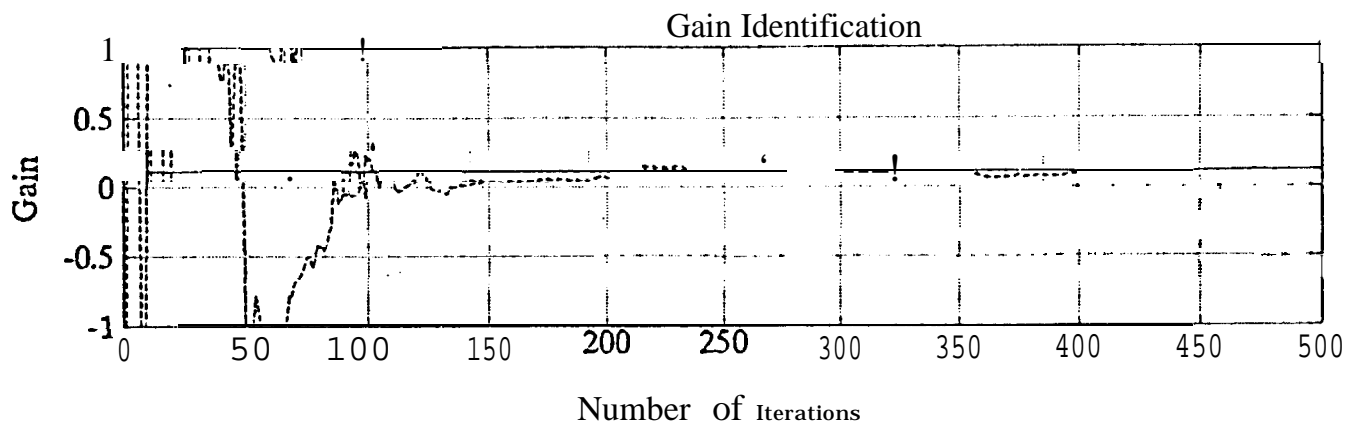


Figure 20. Estimated 5th Modal Gain of the Reduced Order System.

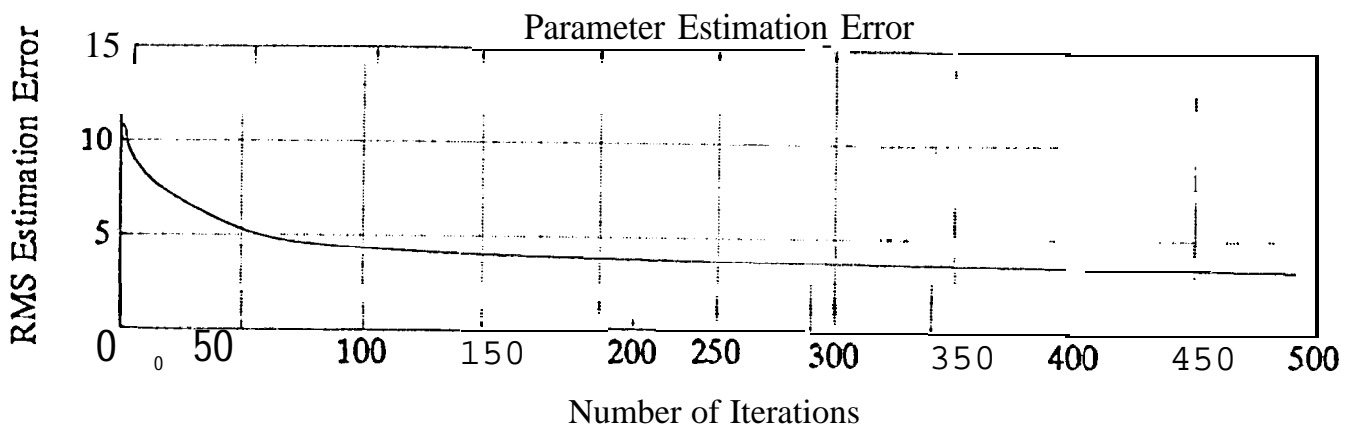


Figure 21. RMS Value of 5th Modal Parameter Estimation Error.

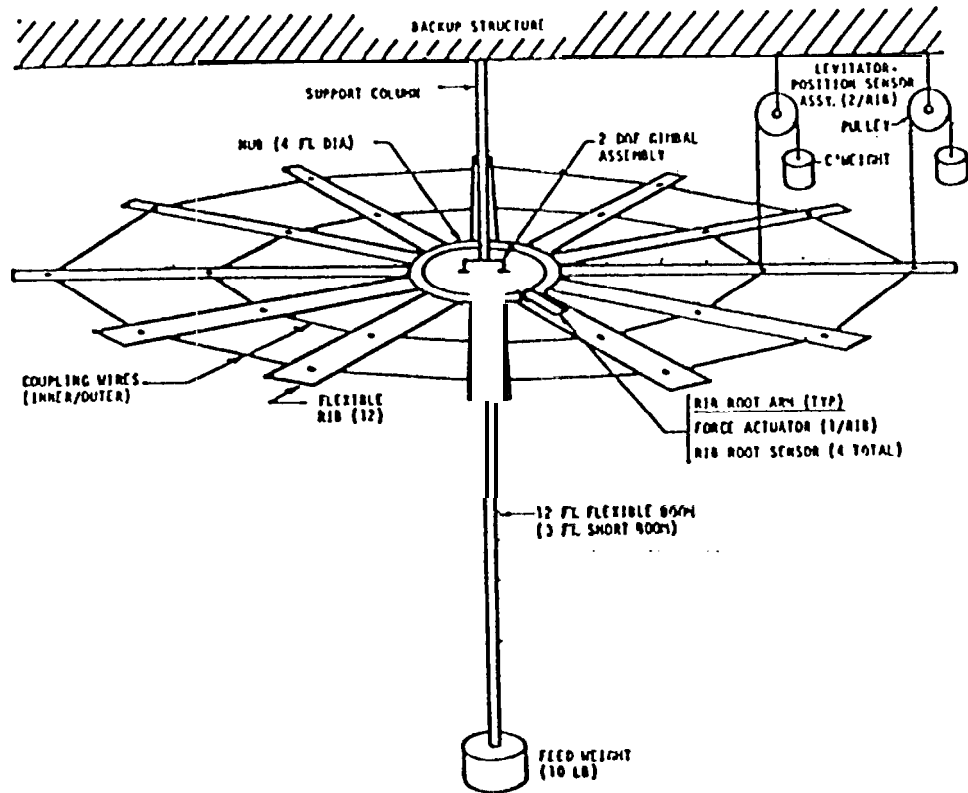


Figure 22. Schematic of the Experiment Structure.

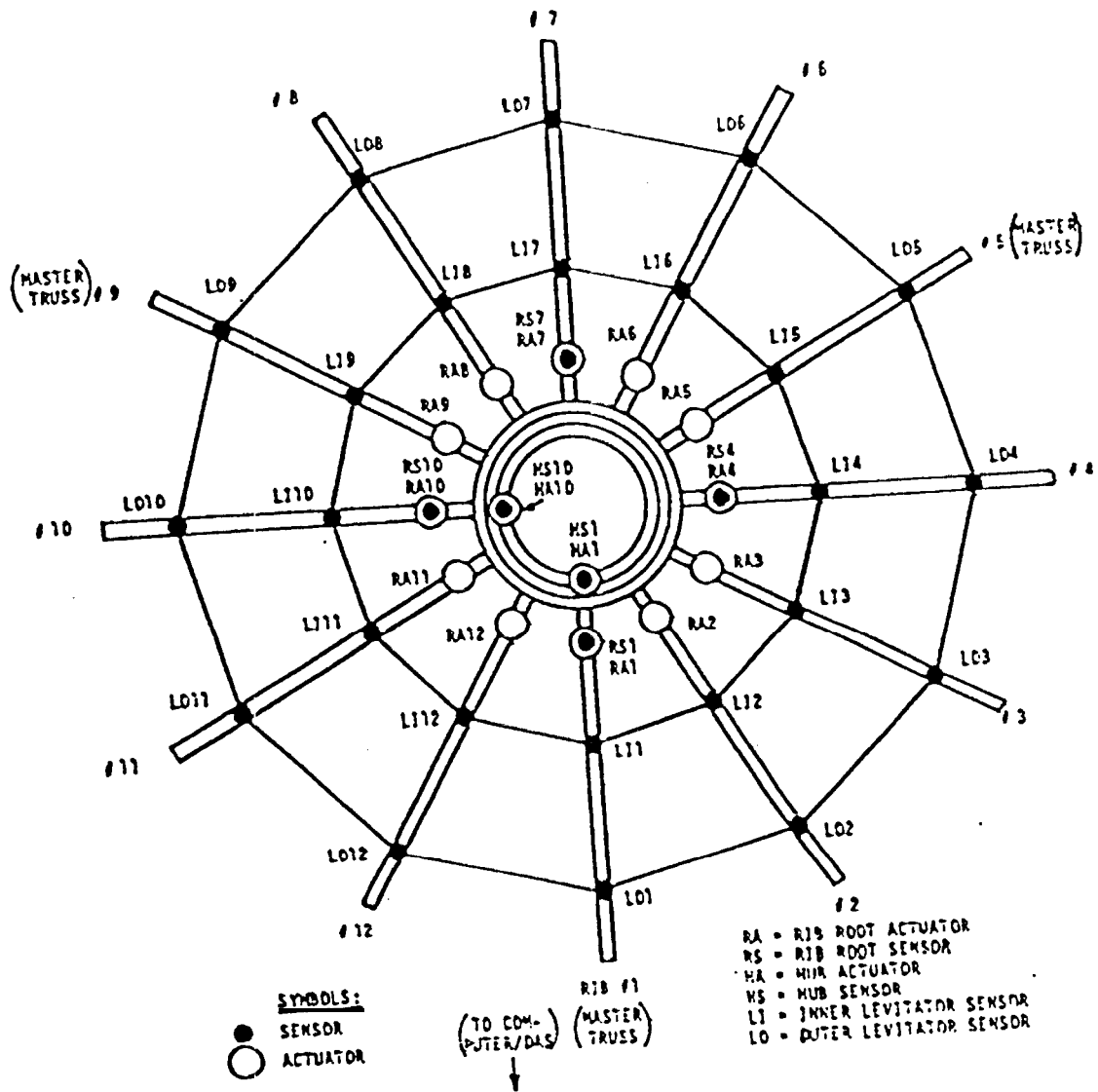


Figure 23. Transducer Location and Labeling - Plan View